

Gaussian Process Bandit Optimization with Machine Learning Predictions and Application to Hypothesis Generation

Xin Jennifer Chen ^{*1} Yunjin Tong ^{*2}

Abstract

Many real-world optimization problems involve an expensive ground-truth oracle (e.g., human evaluation, physical experiments) and a cheap, low-fidelity prediction oracle (e.g., machine learning models, simulations). Meanwhile, abundant offline data (e.g., past experiments and predictions) are often available and can be used to pre-train powerful predictive models, as well as to provide an informative prior. We propose Prediction-Augmented Gaussian Process Upper Confidence Bound (PA-GP-UCB), a novel Bayesian optimization algorithm that leverages both oracles and offline data to achieve provable gains in sample efficiency for the ground-truth oracle queries. PA-GP-UCB employs a control-variates estimator derived from a joint Gaussian process posterior to correct prediction bias and reduce uncertainty. We prove that PA-GP-UCB preserves the standard regret rate of GP-UCB while achieving a strictly smaller leading constant that is explicitly controlled by prediction quality and offline data coverage. Empirically, PA-GP-UCB converges faster than Vanilla GP-UCB and naïve prediction-augmented GP-UCB baselines on synthetic benchmarks and on a real-world hypothesis evaluation task grounded in human behavioral data, where predictions are provided by large language models. These results establish PA-GP-UCB as a general and sample-efficient framework for hypothesis generation under expensive feedback.

1. Introduction

Many real-world optimization problems, ranging from scientific discovery and engineering design to creative content

^{*}Equal contribution (in alphabetical order). ¹Department of Management Science and Engineering, Stanford University, Stanford, USA ²Graduate School of Business, Stanford University, Stanford, USA. Correspondence to: Yunjin Tong <yj-tong@stanford.edu>.

generation, require exploring high-dimensional, continuous spaces to find inputs that maximize an unknown objective function (Frazier, 2018; Shahriari et al., 2015; Snoek et al., 2012). It is common in these settings to have the presence of two complementary information sources: an expensive, high-fidelity oracle (e.g., human evaluation, physical experiment, or high-accuracy simulation) that provides accurate but costly feedback, and a cheap, low-fidelity prediction (e.g., a machine learning model, coarse simulation, large language models (LLMs) or analytical approximation) that gives fast but potentially biased estimates (Forrester & Keane, 2009; Kandasamy et al., 2016; Peherstorfer et al., 2018). The low-fidelity prediction oracle is especially relevant given the rise in the capability of LLMs (Brown et al., 2020; Kaplan et al., 2020).

Meanwhile, in many applications, abundant offline data, collected from past experiments, historical records, or under different experimental conditions, can be leveraged to pre-train predictive models and construct informative priors (Bai et al., 2023). This has renewed interest in hybrid pipelines where models guide search but high-fidelity evaluation remains the decision bottleneck. More recently, researchers have begun using AI systems to prioritize hypotheses for follow-up study (Ludwig & Mullainathan, 2024), and labs report using LLMs as lightweight prediction oracles in scientific workflows (Anthropic, 2026). On the other hand, most practitioners still rely on high-fidelity oracles to ensure the reliability of their optimization results (Diessner et al., 2022; Brochu et al., 2010). The key question is how to optimally combine online expensive feedback with both an inexpensive prediction and existing offline data to efficiently navigate the search space and converge to the optimum with minimal use of the expensive oracle (Wang et al., 2024; Foumani et al., 2023). This problem fundamentally calls for a Bayesian sequential decision-making framework that can formalize prior knowledge, propagate model uncertainty, and support provable exploration-exploitation trade-offs under costly evaluations.

Gaussian process (GP) bandit algorithms, such as Gaussian Process Upper Confidence Bound (Vanilla GP-UCB) (Srinivas et al., 2010), provide such a framework for global optimization of unknown functions in continuous domains

(Williams & Rasmussen, 2006). By modeling the objective with a GP and sequentially selecting query points that balance exploration and exploitation, Vanilla GP-UCB achieves sublinear cumulative regret with high probability. However, Vanilla GP-UCB relies solely on the expensive online oracle and does not leverage cheap prediction information or offline data that may be available in many applications. This limitation motivates the development of methods that can incorporate prediction data and offline observations to accelerate optimization while maintaining theoretical guarantees.

Meanwhile, a complementary line of work explores how to leverage biased but informative predictions in statistical inference and decision-making. Prediction-Powered Inference (PPI) (Angelopoulos et al., 2023) provides a general framework for incorporating offline-trained predictive models via bias correction using limited ground-truth data, but it is designed for static inference rather than sequential learning. A follow-up work by (Ji et al., 2025) extends this idea to sequential decision-making, where the Machine Learning-Assisted Upper Confidence Bound (MLA-UCB) algorithm uses machine-learned predictions to accelerate exploration in discrete multi-armed bandits. However, these approaches are restricted to discrete action spaces and do not exploit structural relationships between arms, nor do they address how to jointly combine predictions, offline data, and expensive online feedback in continuous domains, such as those arising in hypothesis generation tasks.

We propose Prediction-Augmented Gaussian Process Upper Confidence Bound (PA-GP-UCB), a novel algorithm that extends the GP-UCB framework to settings with both an expensive ground-truth oracle and a cheap, low-fidelity prediction oracle, together with offline data. To leverage the statistical relationship between these information sources, PA-GP-UCB models the high-fidelity ground-truth function and the low-fidelity prediction as correlated tasks under a multi-task Gaussian process prior. The algorithm proceeds in two stages. In the offline stage, PA-GP-UCB acquires low-cost prediction oracles over a uniform, space-filling design, using existing offline data or by making queries to the prediction oracle. In the online stage, the algorithm sequentially queries the expensive oracle while obtaining corresponding low-fidelity predictions at the same query points. At each iteration, PA-GP-UCB integrates low-fidelity predictions with high-fidelity observations through a control-variates estimator, enabling variance reduction and bias correction. The next query point is then selected by maximizing an upper confidence bound derived from this fused estimator. In contrast to classical multi-fidelity bandit formulations (Forrester et al., 2007; Kandasamy et al., 2016), we treat predictions as effectively free side information rather than alternative query fidelities.

The PA-GP-UCB method is general and applicable to con-

tinuous optimization problems involving two information sources with different costs and fidelities. While PA-GP-UCB can naturally leverage offline data when such data are available, it does not strictly rely on historical datasets; in the absence of prior data, offline information can instead be generated using predictive sources such as learned models or LLMs. Our main contributions are as follows:

- We introduce PA-GP-UCB, a Gaussian process bandit algorithm that leverages expensive and cheap oracles together with offline data via a novel control-variates estimator, enabling principled variance reduction and bias correction.
- We provide a theoretical analysis of PA-GP-UCB, showing that it achieves a cumulative regret bound that improves upon Vanilla GP-UCB by a constant factor explicitly controlled by the prediction correlation and offline data coverage, and empirically validate these gains on synthetic Gaussian process benchmarks.
- We present PA-GP-UCB as a general framework for sample-efficient hypothesis generation under expensive feedback, and demonstrate its effectiveness on a real-world hypothesis evaluation task grounded in human behavioral data, where it efficiently uncovers high-quality hypotheses using predictions from LLMs.

PA-GP-UCB provides a novel framework for sample-efficient hypothesis generation in settings with expensive feedback. In this setting, the expensive oracle corresponds to human evaluation or physical experimentation, while cheap, low-fidelity predictions are provided by LLMs (Zhou et al., 2024; Forrester et al., 2007). By maximizing the upper confidence bound of a bias-corrected posterior, PA-GP-UCB naturally proposes novel candidate hypotheses while improving the efficiency of hypothesis evaluation, enabling extrapolation beyond the initial set of human-proposed ideas. To our knowledge, it is the first systematic framework that enables principled, integrated hypothesis generation and efficient evaluation by leveraging predictions in embedded continuous hypothesis spaces. This framework is particularly well suited to scientific hypothesis generation, where hypotheses exhibit meaningful structure, data are limited, and predictive models may be imperfect. Details of this application and the corresponding experimental results are presented in Section 6. A more detailed discussion of related work is provided in Appendix A.

2. Problem Statement and Preliminaries

Consider the problem of optimizing an unknown true reward function $f \equiv f^{\text{true}} : \mathcal{X} \mapsto \mathbb{R}$, where $\mathcal{X} \subseteq [0, r]^d$ is a compact and convex set. We have two noisy function value oracles $y^i : \mathcal{X} \mapsto \mathbb{R}$ for $i \in \{\text{true, ML}\}$. The ground-truth

oracle $y(x) \equiv y^{\text{true}}(x) = f(x) + \varepsilon$ is a noisy observation of the true reward function, with the independent observation noise $\varepsilon \sim \mathcal{N}(0, \eta^2)$. The machine-learning-prediction oracle (which we refer to as the ML oracle or the prediction oracle) outputs noisy observations of $f^{\text{ML}} : \mathcal{X} \mapsto \mathbb{R}$, which is a potentially biased machine learning prediction of f . In particular, $y^{\text{ML}}(x) = f^{\text{ML}}(x) + \varepsilon_{\text{ML}}$ with $\varepsilon_{\text{ML}} \sim \mathcal{N}(0, \eta_{\text{ML}}^2)$, with ε_{ML} and ε independent of each other and of f^{ML} .

We consider the two-stage offline-online setting. In the offline stage, only the prediction oracle can be accessed a finite number of times. We refer to the offline dataset as $\mathcal{D}^{\text{off}} = \{(x_i, y^{\text{ML}}(x_i))\}_{i \in [n_{\text{off}}]}^1$, and the algorithm can decide n_{off} how many points and which points to query. The online stage proceeds sequentially with a finite horizon T – at each round t , when querying a point, both oracles are observed by the algorithm, and the algorithm picks the next point to query, repeatedly for T rounds. Let $\mathcal{D}_t = \{(x_i, y(x_i), y^{\text{ML}}(x_i))\}_{i \in [t]}$ denote the online dataset up to round t . This setting mirrors common practical scenarios where the true reward function is expensive to evaluate and must therefore be optimized sequentially, while a cheap prediction oracle can be queried at scale ahead of time. Observing both oracles online is natural because once an expensive query is made at a point, the marginal cost of computing the prediction at the same point is negligible, enabling the algorithm to exploit cross-source correlation throughout learning.

Objective The goal of this paper is to maximize cumulative reward $\sum_{t=1}^T f(x_t)$, which can be interpreted as aiming to perform as well as $x_* = \arg \max_{x \in \mathcal{X}} f(x)$. Cumulative regret is a natural performance metric for this goal. After an algorithm is run for T rounds, the cumulative regret is $R_T \triangleq \sum_{t \in [T]} [f(x_*) - f(x_t)] = \sum_{t \in [T]} r_t$, and we define $r_t = f(x_*) - f(x_t)$ as the instantaneous regret in round t .

Gaussian Process Model We model the true and ML-predicted reward functions jointly as a sample from a two-output Gaussian process:

$$\begin{bmatrix} f \\ f^{\text{ML}} \end{bmatrix} \sim \mathcal{GP} \left(\begin{bmatrix} 0 \\ 0 \end{bmatrix}, K(x, x') \otimes B \right), \quad B = \begin{bmatrix} 1 & \rho \\ \rho & 1 \end{bmatrix}.$$

It is necessary to impose some structural property on the GP kernel in a compact domain setting, and we consider the following, which is identical to the classical GP bandits setting in (Srinivas et al., 2010).

Assumption 2.1. For some constants $a, b > 0$,

$$\mathbb{P} \left[\sup_{x \in \mathcal{X}} \left| \frac{\partial f^i}{\partial x_j} \right| > L \right] \leq a e^{-(L/b)^2}, \quad j \in [d], i \in \{\text{true, ML}\}.$$

¹We adopt the common notation that $[k] = \{1, 2, \dots, k\}$.

If set $L = b\sqrt{\log(da/\delta)}$, then we get with probability greater than $1 - \delta$,

$$|f^i(x) - f^i(x')| \leq L \|x - x'\|_1, \quad \forall x, x' \in \mathcal{X}, i \in \{\text{true, ML}\}.$$

We further restrict to GPs with nonzero and bounded variance $0 < K(x, x) \leq 1$.

Notations To simplify notations, we define the following quantities from the joint posteriors at round $t \in [T]$, $i \in \{\text{true, ML}\}$,

$$\begin{aligned} \mu_t^i(x) &\triangleq \mathbb{E}[f^i(x) | \mathcal{D}_{t-1}], \quad \mu^{\text{off}}(x) \triangleq \mathbb{E}[f^{\text{ML}}(x) | \mathcal{D}^{\text{off}}], \\ \sigma_t^{\text{ML,all}}(x) &\triangleq \mathbb{E}[f^{\text{ML}}(x) | \mathcal{D}^{\text{off}} \cup \mathcal{D}_{t-1}], \\ (\sigma_t^i(x))^2 &\triangleq \text{Var}(f^i(x) | \mathcal{D}_{t-1}), \\ (\sigma_t^{\text{off}}(x))^2 &\triangleq \text{Var}(f^{\text{ML}}(x) | \mathcal{D}^{\text{off}}), \\ (\sigma_t^{\text{ML,all}}(x))^2 &\triangleq \text{Var}(f^{\text{ML}}(x) | \mathcal{D}^{\text{off}} \cup \mathcal{D}_{t-1}), \\ \rho_t(x) &\triangleq \frac{\text{Cov}(f(x), f^{\text{ML}}(x) | \mathcal{D}_{t-1})}{\sigma_t^{\text{true}}(x) \sigma_t^{\text{ML}}(x)}. \end{aligned}$$

3. The PA-GP-UCB Algorithm

This section introduces PA-GP-UCB, with details described in Algorithm 1. When applying the PA-GP-UCB algorithm, we maintain two joint GP models at each round t , the global $\mathcal{GP}_{\text{all}}$ trained on $\mathcal{D}^{\text{off}} \cup \mathcal{D}_{t-1}$, and the online \mathcal{GP} trained on only online data \mathcal{D}_{t-1} .

Offline Stage Design PA-GP-UCB begins with an offline stage, which queries only the prediction oracle on an ε -net² of \mathcal{X} and collects N repeated observations at each grid center. These observations are then used to perform GP updating on $\mathcal{GP}_{\text{all}}$. Repeated queries reduce the effective observation noise from η_{ML}^2 to η_{ML}^2/N at grid center points. Then through a high enough coverage by the ε -net, GP interpolation reduces $\sigma_t^{\text{ML,all}}(x)$ for all $x \in \mathcal{X}$. Note that the offline stage could be parallelized to finish in $\mathcal{O}(1)$ round³.

We summarize the effect of offline prediction coverage by a uniform ratio bound $(\sigma_t^{\text{ML,all}}(x)/\sigma_t^{\text{ML}}(x))^2 \leq R$ for all $x \in \mathcal{X}, t \leq T$. Smaller R means offline data makes the ML-predicted posterior uniformly tighter, and will result in a greater improvement in cumulative regret, described in more detail in Section 4. This turns offline data design

²For $\mathcal{X} \subseteq [0, r]^d$ under the ℓ_∞ metric, an ε -net can be constructed by a uniform grid: partition each coordinate into intervals of width 2ε and include the center of each resulting axis-aligned hypercube. Then for any $x \in \mathcal{X}$ there exists a grid center c with $\|x - c\|_\infty \leq \varepsilon$. The net size is at most $\lceil r/(2\varepsilon) \rceil^d$.

³We measure round complexity under a parallel query model: in one round we issue up to Q oracle queries non-adaptively, with $Q = \mathcal{O}(\text{poly}(d, T))$, and receive all responses simultaneously. Under this model, the offline stage has constant round complexity.

(ε, N) into a knob that directly controls regret constants. In Lemma B.3, we provide detailed sufficient conditions on the offline procedure parameters (ε, N) that guarantee the uniform ratio bound to hold for any selected value of R with high probability. Asymptotically⁴, the sufficient conditions required for any $R \in (0, 1]$ are

$$\varepsilon = \tilde{\mathcal{O}} \left(\sqrt{\frac{R}{T}} \frac{\eta_{\text{ML}}}{d} \right), \text{ and } N = \Omega \left(\frac{T}{R} \right). \quad (1)$$

The sufficient conditions in (1) are worst-case and conservative; Sections 5 and 6 show substantial decrease in cumulative regret even with ε much larger and N much smaller than required by (1).

Online Stage Design To leverage the offline prediction oracle queries in a statistically efficient way, we introduce a control-variates estimator (2) to construct an upper confidence bound for the true reward function used in the online stage:

$$\mu_t^{\text{PA}}(x) \triangleq \mu_t^{\text{true}}(x) - \frac{\rho_t(x)\sigma_t^{\text{true}}(x)}{\sigma_t^{\text{ML}}(x)} (\mu_t^{\text{ML}}(x) - \mu_t^{\text{ML,all}}(x)). \quad (2)$$

PPI-inspired estimators use a model prediction as a baseline and correct it with a mean-zero residual computed from ground-truth labels (Angelopoulos et al., 2023). In our setting, the GP posterior enables an analogous decomposition: the residual $\mu_t^{\text{ML}}(x) - \mu_t^{\text{ML,all}}(x)$ has mean zero conditional on online data, and the GP supplies the optimal (minimum MSE) linear predictor coefficient through $\rho_t(x)\sigma_t^{\text{true}}(x)/\sigma_t^{\text{ML}}(x)$ (Anderson, 2003). Unlike MLA-UCB in the discrete-arm setting (Ji et al., 2025), PA-GP-UCB uses a full probabilistic prediction-augmented posterior over a continuous domain, where the offline data reduces uncertainty globally.

PA-GP-UCB then selects the next point that maximizes the prediction-augmented upper confidence bound:

$$\varphi_t(x) \triangleq \mu_t^{\text{PA}}(x) + \sqrt{\beta_t} \sigma_t^{\text{PA}}(x). \quad (3)$$

It is shown in Lemma B.2 that $(\sigma_t^{\text{PA}}(x))^2$ is equal to

$$(\sigma_t^{\text{true}}(x))^2 \left[\left(\rho_t(x) \frac{\sigma_t^{\text{ML,all}}(x)}{\sigma_t^{\text{ML}}(x)} \right)^2 + 1 - \rho_t(x)^2 \right]. \quad (4)$$

The posterior uncertainty under our algorithm is always weakly smaller than that under the Vanilla GP-UCB algorithm. The online stage of the algorithm uses the same optimism structure as GP-UCB but with a smaller uncertainty achieved by prediction data.

⁴ $\tilde{\mathcal{O}}$ hides polylogarithmic factors (e.g., powers of $\log T, \log d$, etc.).

Algorithm 1 PA-GP-UCB

```

1: Input: domain  $\mathcal{X} \subseteq [0, r]^d$ , radius  $\varepsilon$ , replication  $N$ , prior kernel  $K(\cdot, \cdot)$ , correlation matrix  $B$ , horizon  $T$ .
2: Construct an  $\varepsilon$ -net  $\{c_1, \dots, c_M\} \subset \mathcal{X}$  of size  $M = \lceil \frac{r}{2\varepsilon} \rceil^d$ .
3: for  $i = 1, \dots, M$  do
4:   for  $j = 1, \dots, N$  do
5:     Observe  $y_{ij}^{\text{ML}} \leftarrow y^{\text{ML}}(c_i)$ 
6:      $\mathcal{GP}_{\text{all}} \leftarrow \text{UPDATE}(\mathcal{GP}_{\text{all}}, (c_i, y_{ij}^{\text{ML}}))$ 
7:   end for
8: end for
9: for  $t = 1, 2, \dots, T$  do
10:    $x_t \leftarrow \arg \max_{x \in \mathcal{X}} \varphi_t(x)$ 
11:   Observe  $y_t \leftarrow y(x_t)$ 
12:   Observe  $y_t^{\text{ML}} \leftarrow y^{\text{ML}}(x_t)$ 
13:    $\mathcal{GP}_{\text{all}} \leftarrow \text{UPDATE}(\mathcal{GP}_{\text{all}}, (x_t, y_t, y_t^{\text{ML}}))$ 
14:    $\mathcal{GP} \leftarrow \text{UPDATE}(\mathcal{GP}, (x_t, y_t, y_t^{\text{ML}}))$ 
15: end for

```

4. Theoretical Guarantees

This section presents the cumulative regret analysis of PA-GP-UCB. Our bound matches the standard GP-UCB rate $\tilde{\mathcal{O}}(\sqrt{dT\gamma_T})$, where γ_T is the information gain of using T number of only ground-truth oracle queries (without prediction oracle queries), same as in (Srinivas et al., 2010). See definition of γ_T in (9). Moreover, our algorithm obtains a strictly smaller leading constant whenever the prediction is informative ($\rho \neq 0$) and offline prediction data reduces uncertainty uniformly (isolated in the constant R).

The multiplicative improvement over Vanilla GP-UCB is controlled by the factor $\sqrt{1 - (1 - R)\rho^2}$. It equals 1 (no gain) when $\rho = 0$ or $R = 1$, and approaches 0 (maximal gain) as $\rho \rightarrow 1$, and $R \rightarrow 0$.

Theorem 4.1 (Cumulative Regret Bound). *If Assumption 2.1 holds, and suppose the offline data satisfy the uniform ratio condition*

$$(\sigma_t^{\text{ML,all}}(x)/\sigma_t^{\text{ML}}(x))^2 \leq R$$

for some $R \in (0, 1]$.

Let $\beta_t = 2 \log(2\pi^2 t^2/(3\delta)) + 4d \log(dtbr \sqrt{\log(4da/\delta)})$, $C_1 = 8/\log(1 + ((\eta^2 + \rho^2 \eta_{\text{ML}}^2)/(1 - \rho^2))^{-1})$. Then with probability $\geq 1 - \delta$, PA-GP-UCB satisfies for all $T \geq 1$,

$$R_T \leq \sqrt{C_1 \beta_T T [1 - (1 - R)\rho^2] \gamma_T} + \frac{\pi^2}{6}.$$

Proof. Theorem 4.1 is proved in Appendix B. \square

When applying the Vanilla UCB-GP algorithm described in (Srinivas et al., 2010), the cumulative regret under the

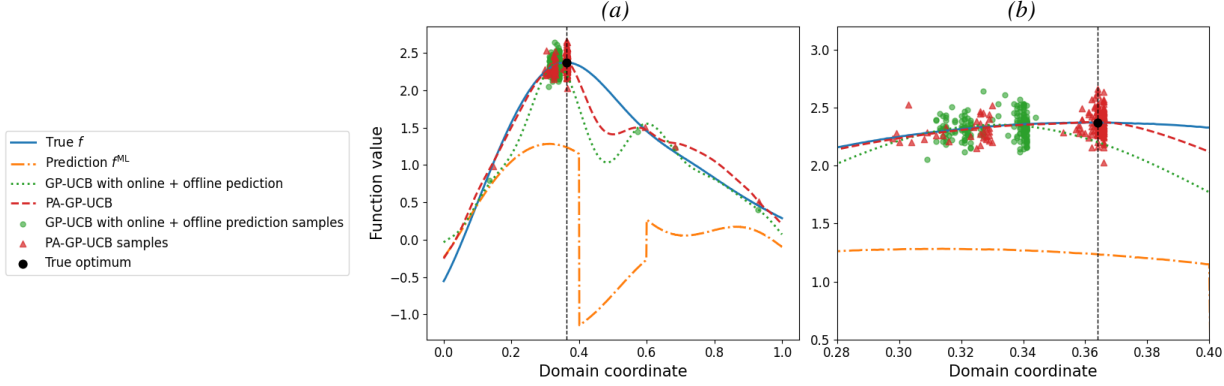


Figure 1. (a) Posterior means at $T = 200$ for PA-GP-UCB and naïve prediction-augmented GP-UCB compared with the ground-truth function f and the locally anti-correlated prediction f^{ML} . (b) Zoomed-in view around the true optimum, highlighting that PA-GP-UCB concentrates samples near the optimum while naïve prediction-augmented GP-UCB remains biased toward the prediction-preferred region.

same assumptions is guaranteed to have the following for all $T \geq 1$,

$$R_T^{\text{Vanilla}} \leq \sqrt{C_2 T \beta_T \gamma_T} + \frac{\pi^2}{6}, \quad C_2 = \frac{8}{\log(1 + \eta^{-2})}.$$

Corollary 4.2 (Strictly Better Performance). *Let $R^* \triangleq \min \left\{ \frac{\frac{C_2}{C_1} - (1 - \rho^2)}{\rho^2}, 1 \right\}$. When $R < R^*$ and $\rho \neq 0$, then running Vanilla GP-UCB algorithm gives a cumulative regret strictly larger than that after running PA-GP-UCB, i.e. for all $T \geq 1$,*

$$R_T^{\text{Vanilla}} > R_T.$$

An asymptotic and with-high-probability conservative sufficient condition is

$$\varepsilon = \tilde{\mathcal{O}} \left(\sqrt{\frac{R^*}{T} \frac{\eta_{\text{ML}}}{d}} \right), \text{ and } N = \Omega \left(\frac{T}{R^*} \right). \quad (5)$$

In practice, one chooses an offline budget/design (e.g., ε -net size and replication N , or alternative non-uniform designs) that is computationally feasible, and can empirically estimate the induced \hat{R} on a holdout set by comparing $\sigma_t^{\text{ML,all}}(x)$ and $\sigma_t^{\text{ML}}(x)$ for x in the holdout set. Corollary 4.2 can then be read as: whenever $\hat{R} < R^*$, PA-GP-UCB provably improves the regret constant. Our experiments in later sections show substantial regret reductions even with much larger ε and smaller N than (5), consistent with the fact that (5) is extremely conservative and that performance depends on the variance reduction achieved at the points actually explored by the algorithm, rather than worst-case uniform coverage.

5. Numerical Analysis

We first validate PA-GP-UCB on synthetic data to examine its efficiency and bias correction under controlled conditions.

We generate a ground-truth function f by sampling from a one-dimensional Gaussian process with an RBF kernel over a domain $D \subseteq [0, 1]$. To construct a correlated but biased prediction, we draw an independent GP sample g from the same kernel and define $f^{\text{ML}} = \rho f + \sqrt{1 - \rho^2} g$, which we use as the prediction with controllable correlation ρ to the ground truth. At each iteration, the algorithm queries both the human oracle and the prediction oracle with different noise variances and updates a joint two-task GP posterior.

5.1. Comparison to Naïve Prediction-Augmented Baselines

In addition to Vanilla GP-UCB, we consider two naïve prediction-augmented baselines: (i) GP-UCB with offline prediction data, which incorporates only pre-collected prediction observations into the GP prior, and (ii) GP-UCB with offline and online prediction data, which augments the GP with both offline predictions and prediction observations collected online but does not correct for prediction bias. These baselines allow us to separately evaluate the contribution of variance reduction from prediction data and the additional benefit of explicit bias correction.

To evaluate robustness under structured prediction misspecification, we construct a synthetic setting in which the predictions are globally correlated with the true objective but locally misleading. Specifically, we flip the sign of the prediction within a sub-interval $[0.4, 0.6]$, i.e., $f^{\text{ML}}(x) \leftarrow -f^{\text{ML}}(x)$ in this region. This preserves global correlation while inducing a localized regime in which the prediction is confidently anti-correlated with the true objective. Figure 1 and Figure 2(a) show that GP-UCB augmented with offline, or offline and online, prediction data initially achieves relatively low cumulative regret by exploiting prediction guidance, but its posterior remains biased toward the prediction-preferred region and fails to recover

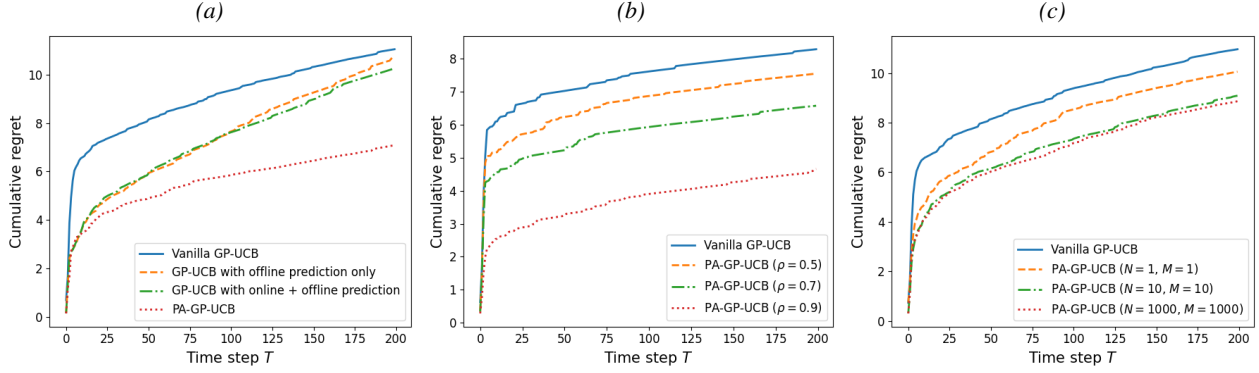


Figure 2. Cumulative regret of Vanilla GP-UCB, naïve prediction-augmented GP-UCB baselines, and PA-GP-UCB, averaged over 50 runs with horizon $T = 200$. (a) Comparison of Vanilla GP-UCB, GP-UCB with offline predictions only, GP-UCB with both online and offline predictions, and PA-GP-UCB under $\rho = 0.8$, $\eta^2 = \eta_{\text{ML}}^2 = 0.01$, and $M = N = 1000$. (b) Effect of correlation $\rho \in \{0.5, 0.7, 0.9\}$ with $\eta^2 = \eta_{\text{ML}}^2 = 0.001$ and $M = N = 1000$. (c) Effect of varying the offline prediction data sizes M and N with $\eta^2 = \eta_{\text{ML}}^2 = 0.01$.

the true optimum. In contrast, PA-GP-UCB uses online prediction feedback to estimate local correlation and explicitly correct the prediction-induced shift in the human posterior, enabling it to reallocate exploration toward the true optimum and achieve both lower asymptotic regret and accurate localization of the optimum.

5.2. Ablation on Prediction Correlation and Offline Coverage

Figure 2(b) shows that PA-GP-UCB consistently outperforms Vanilla GP-UCB across all correlation levels. Notably, even with moderate correlation ($\rho = 0.5$), PA-GP-UCB achieves substantial improvements, indicating that strong alignment between predictions and the ground-truth objective is not required in practice. Higher values of ρ further amplify this advantage by enabling more effective information transfer from the offline predictor.

Figure 2(c) varies the number of offline ε -net size M and repetitions N . PA-GP-UCB outperforms Vanilla GP-UCB across all settings, including the minimal regime $M = N = 1$, suggesting that even a very small amount of offline prediction data is sufficient to yield meaningful performance gains in practice, without requiring the strong conditions assumed by the theoretical guarantees. Increasing M and N further improves performance by reducing posterior uncertainty in the prediction oracle.

Further posterior visualizations illustrating the temporal evolution of PA-GP-UCB are provided in Appendix D.1. Additional ablation studies examining the effects of observation noise and prediction noise are reported in Appendix D.2.

6. Application to Hypothesis Generation

We now apply PA-GP-UCB to the problem of hypothesis generation, where the goal is to discover high-quality hy-

potheses with minimal human feedback or evaluation of the ground truth. Each hypothesis corresponds to a point x in a continuous embedding space $\mathcal{X} \subset \mathbb{R}^d$ (e.g., the latent representation of a scientific idea, design concept, or policy proposal). A human oracle provides expensive, noisy ground-truth feedback $f(x)$, while machine learning predictions (e.g., LLMs) provide cheap, biased predictions $f^{\text{ML}}(x)$. The key challenge is to efficiently explore \mathcal{X} and converge to the hypothesis that maximizes the ground truth function, using the prediction to accelerate exploration while correcting for its bias (Zhou et al., 2024). PA-GP-UCB is particularly well-suited for this task because it naturally generates novel candidate hypotheses by maximizing the UCB of the bias-corrected posterior, enabling extrapolation beyond the initial set of human-proposed ideas. By combining human anchoring with prediction-accelerated exploration, PA-GP-UCB provides an efficient framework for human–AI co-discovery with provably faster convergence than standard GP-UCB.

We evaluate PA-GP-UCB in two complementary environments, both grounded in the real human behavioral dataset of (Milkman et al., 2021). The dataset contains large-scale field measurements of how different experimental messaging conditions influence user visitation behavior. We compute the mean human visitation reward for each experimental condition: $f(a_i) = \mathbb{E}[\text{visits} \mid \text{exp_condition} = a_i], i = 1, \dots, n$. This yields $n = 54$ distinct human-defined “arms” $\{a_i\}$ with corresponding ground-truth human outcomes. These same arms form the basis of our two evaluation settings. First, in a finite-arm setting, the algorithm operates directly on the 54 discrete human-measured hypotheses, yielding a bandit problem with no underlying smoothness structure. Second, we construct a human-derived synthetic environment, a structure-preserving continuous benchmark obtained by embedding the same 54 arms into a two-dimensional semantic manifold and smoothing their human

reward values into a continuous function.

6.1. Finite-Arm Hypothesis Evaluation

We treat the set of hypotheses for which we have real experimental outcomes as a finite action set $\mathcal{A} = \{x_1, \dots, x_n\}$, where each x_i is an embedding of an intervention or hypothesis description. We define $f(x_i) = f(a_i), i = 1, \dots, n$ treating the collected experimental data as the true underlying human feedback function. We construct f^{ML} using a lightweight regression model trained on the embedding space, where only half of the arms are visible during training and, for those visible arms, only half of their observations are used. This mimics the real-world scenarios where f^{ML} takes less information and is correlated to f with bias. The regret is computed with respect to the best human-evaluated hypothesis $x^* = \arg \max_{x_i \in \mathcal{A}} f(x_i)$ and $R_T = \sum_{t=1}^T (f(x^*) - f(x_t))$.

6.1.1. RESULTS

Across the 54 experimental conditions, the prediction model achieves a moderate empirical correlation of $\hat{\rho} = 0.66$ with the ground-truth human reward. Figure 3(a) shows cumulative regret over $T = 200$ for PA-GP-UCB with varying numbers of offline prediction duplicates (1, 10, and 100). Across all settings, PA-GP-UCB exhibits substantially lower sublinear regret than Vanilla GP-UCB. The performance gap widens as the number of offline prediction duplicates increases, since additional prediction observations provide stronger global structure and reduce posterior uncertainty in regions where human data are sparse. Notably, even though $\hat{\rho}$ is an empirical estimate that may vary with x , using this estimated correlation is sufficient to significantly reduce regret, highlighting the robustness of PA-GP-UCB to heterogeneous prediction alignment.

In this discrete bandit setting, the true reward is highly non-smooth and does not admit a meaningful GP structure, causing Vanilla GP-UCB to exhibit large posterior uncertainty and unstable exploration. PA-GP-UCB instead leverages a noisy but globally informative prediction model to impose latent structure over the action space. The resulting two-task GP reduces posterior variance early, while the control-variates estimator debiases the prediction and balances information across tasks, yielding more stable exploration and faster convergence despite the discrete, non-GP nature of the reward.

6.2. Structure-Preserving Continuous Hypothesis Evaluation

To construct a realistic yet fully controllable benchmark, we build a continuous two-dimensional environment directly from the real human evaluation dataset. This pre-

serves the semantic geometry of human hypotheses while enabling dense sampling and closed-form regret computation. Each arm description a_i is embedded through a TF-IDF vectorizer (Salton & Buckley, 1988) with bi-grams $v_i = \text{TFIDF}(a_i) \in \mathbb{R}^d$. We reduce the TF-IDF vectors to a human-structured two-dimensional manifold $x_i = \text{UMAP}(v_i) \in [0, 1]^2$ via UMAP (McInnes et al., 2020). The embedding is rescaled to $[0, 1]^2$ along each dimension. UMAP clusters semantically similar interventions into coherent regions and produces a low-dimensional manifold enabling generalization beyond the 54 observed arms. This construction relies only on corpus-local statistics, avoiding pretrained semantic embeddings (e.g., word2vec or sentence transformers) that could introduce additional inductive bias.

We fit a Gaussian process $f(x) \sim \mathcal{GP}\left(0, \sigma_f^2 \exp\left(-\frac{1}{2\ell^2} \|x - x'\|^2\right)\right)$ to the 54 human-labeled points $\{(x_i, f(a_i))\}$. The GP posterior mean, evaluated on a dense 100×100 grid $D_{\text{grid}} = \{x_1, \dots, x_M\} \subset [0, 1]^2, M = 10,000$, serves as the continuous human reward function $f^{\text{GP}}(x)$. To construct a cheap but imperfect auxiliary model, we use a LLM (OpenAI o4-mini model (OpenAI, 2025)) as a predictor of human reward. For each arm x_i , we define $f^{\text{ML}}(x_i) \triangleq \mathbb{E}_{\text{LLM}}[\text{predicted visits} \mid \text{prompt}(x_i)]$, where the expectation is approximated by a single fixed-prompt LLM query (the full prompt templates are provided in Appendix E). We consider three prediction variants based on the amount of ground-truth information provided via in-context prompting: (i) a K -shot calibrated prediction with $K = 4$ ground-truth examples, (ii) a stronger K -shot prediction with $K = 12$ examples, and (iii) a scale-only prediction that receives only global summary statistics (min, max, mean) without labeled examples. Each variant induces a biased but informative predictor with increasing alignment to the human reward as K grows. Across all three variants, $\text{corr}(f^{\text{ML}}, f^{\text{GP}}) \approx 0.8$, indicating that the prediction is informative but systematically inaccurate.

The true optimum of the ground-truth GP surface and the cumulative regret are $x^* = \arg \max_{x \in D_{\text{grid}}} f^{\text{GP}}(x)$ and $R_T = \sum_{t=1}^T (f^{\text{GP}}(x^*) - f^{\text{GP}}(x_t))$. Given the best point x_{best} discovered by PA-GP-UCB on the continuous grid, we map it back to a set of nearby real experimental conditions. Specifically, we find the indices of the k closest arms in the 2-D UMAP embedding: $\mathcal{N}_k(x_{\text{best}}) = \left\{ i \in \{1, \dots, n\} : x_i \text{ is among the } k \text{ nearest neighbors of } x_{\text{best}} \right\}$. We then take the original textual descriptions $\{a_i : i \in \mathcal{N}_k(x_{\text{best}})\}$ and prompt an LLM to summarize the common structure and strategy they represent (e.g., shared targeting rules, interventions, or messaging patterns). This produces an interpretable, human-readable explanation of the hypothesis H^*

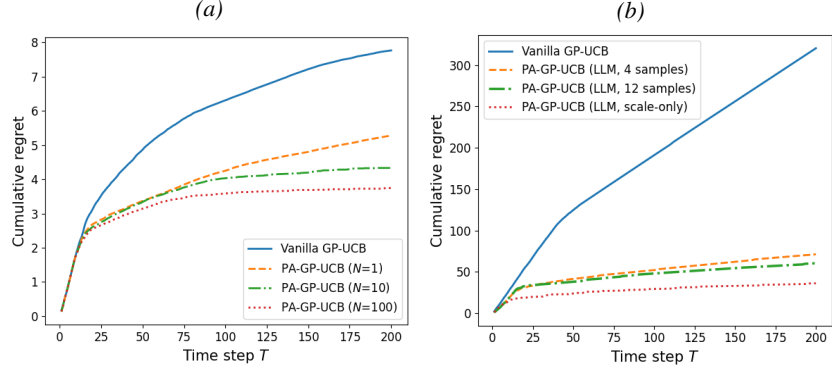


Figure 3. Cumulative regret over horizon $T = 200$, averaged over 50 independent runs. (a) Finite-arm setting: comparison between Vanilla GP-UCB and PA-GP-UCB for different numbers of offline prediction duplicates $N \in \{1, 10, 100\}$, with $\eta^2 = \eta_{ML}^2 = 0.001$ and $\hat{\rho} = 0.66$. (b) Continuous setting: comparison between Vanilla GP-UCB and PA-GP-UCB using an LLM-based prediction, where the prediction is conditioned on different numbers of ground-truth examples via in-context prompting, with $\eta^2 = \eta_{ML}^2 = 0.001$ and $\hat{\rho} = 0.8$.

that PA-GP-UCB discovers in the continuous environment.

6.2.1. RESULTS

Mapping the PA-GP-UCB optimum x_{best} back to the discrete arms reveals its $k = 6$ nearest neighbors: *Higher Incentives a, Higher Incentives b, Gain-Framed Micro-Incentives, Choice of Gain- or Loss-Framed Micro-Incentives, Loss-Framed Micro-Incentives, and Planning, Reminders & Micro-Incentives to Exercise*, which is consistent with the ground-truth human outcomes.

H^* : Interventions that combine relatively large, frequent, performance-contingent monetary incentives, together with basic planning and reminder scaffolding, are especially effective at increasing gym visits.

Figure 3(b) shows cumulative regret for Vanilla GP-UCB and PA-GP-UCB under different LLM prediction variants. Increasing the number of ground-truth examples used to calibrate the prediction improves performance, indicating that better prediction alignment yields more efficient exploration. Notably, the scale-only prediction performs best, as it provides reliable global magnitude information without overfitting to a small labeled set. Notably, Vanilla GP-UCB exhibits nearly linear regret due to posterior misspecification arising from a mismatch between the GP kernel and the latent semantic geometry of the reward function, whereas PA-GP-UCB achieves stable, sublinear regret by regularizing posterior uncertainty with a correlated auxiliary signal through a prediction-informed two-task GP, making it substantially less sensitive to kernel misspecification.

More generally, PA-GP-UCB operates over an abstract optimization space \mathcal{X} and does not require explicit dimensionality reduction or lossy embeddings. Hypotheses may be high-dimensional or discrete, provided an encoding defines a similarity structure and admits exact decoding. This makes the framework particularly well suited to scientific

hypothesis generation, where structured hypotheses induce meaningful geometry, data are sparse, models are often misspecified, and prediction-augmented uncertainty reduction offers substantial gains over standard bandit methods.

7. Conclusions

We propose PA-GP-UCB, a GP bandit algorithm that integrates a cheap but biased prediction oracle and offline data to obtain provable gains in sample efficiency. Under standard GP-UCB assumptions, PA-GP-UCB preserves the usual $\tilde{\mathcal{O}}(\sqrt{T\beta_T\gamma_T})$ regret rate while achieving a strictly smaller leading constant, explicitly controlled by prediction quality and offline data coverage. Empirically, PA-GP-UCB converges faster than Vanilla GP-UCB and naïve prediction-augmented GP-UCB baselines on synthetic benchmarks. We further demonstrate its utility as a novel framework for hypothesis generation through experiments grounded in real human outcomes. In this setting, PA-GP-UCB provides a principled, end-to-end integration of hypothesis generation and evaluation in embedded continuous hypothesis spaces.

One open question is whether the sufficient conditions on (ε, N) can be significantly weakened, as they are conservative and likely not sample-optimal. These conditions are most relevant when offline predictions are orders of magnitude cheaper than online evaluations and can be heavily parallelized. A key direction for future work is improving offline data efficiency, for example via adaptive or non-uniform designs or guarantees based on trajectory-dependent variance reduction rather than a uniform worst-case R . Additional directions include theoretical guarantees of robustness to kernel and prediction misspecification, cost-aware offline sampling that optimizes the offline–online tradeoff, and applications to large-scale scientific hypothesis generation problems with scarce and expensive human evaluation.

Impact Statement

This work advances the field of machine learning with a focus on Bayesian optimization, prediction-augmented algorithms, and Gaussian process bandit optimization. By improving online sample efficiency and reducing reliance on expensive evaluations, the proposed methods have the potential to lower time, computational, and resource costs in real-world applications such as scientific experimentation, engineering design, and human-in-the-loop decision-making. More efficient optimization procedures can enable faster scientific discovery, reduce experimental waste, and make resource-intensive workflows more accessible. While the techniques developed in this paper are methodological in nature, their broader impact lies in supporting more efficient and responsible use of costly human, computational, and physical resources across a range of domains. The methodologies developed in this paper do not raise specific ethical concerns beyond those commonly associated with the responsible use of machine learning systems.

References

Anderson, T. W. *An Introduction to Multivariate Statistical Analysis*. Wiley, 3 edition, 2003.

Angelopoulos, A. N., Bates, S., Fannjiang, C., Jordan, M. I., and Zrnic, T. Prediction-powered inference. *Science*, 382 (6671):669–674, 2023.

Anthropic. How scientists are using claude to accelerate research and discovery, Jan 15 2026. URL <https://www.anthropic.com/news/accelerating-scientific-research>. Accessed: 2026-01-25.

Athey, S., Chetty, R., Imbens, G. W., and Kang, H. The surrogate index: Combining short-term proxies to estimate long-term treatment effects more rapidly and precisely. *Review of Economic Studies*, pp. rda087, 2025.

Auer, P. Using confidence bounds for exploitation-exploration trade-offs. *Journal of machine learning research*, 3(Nov):397–422, 2002.

Auer, P., Cesa-Bianchi, N., Freund, Y., and Schapire, R. E. The nonstochastic multiarmed bandit problem. *SIAM journal on computing*, 32(1):48–77, 2002.

Bai, T., Li, Y., Shen, Y., Zhang, X., Zhang, W., and Cui, B. Transfer learning for bayesian optimization: A survey. *arXiv preprint arXiv:2302.05927*, 2023.

Bogunovic, I., Scarlett, J., and Cevher, V. Time-varying gaussian process bandit optimization. In *Artificial Intelligence and Statistics*, pp. 314–323. PMLR, 2016.

Brochu, E., Cora, V. M., and De Freitas, N. A tutorial on bayesian optimization of expensive cost functions, with application to active user modeling and hierarchical reinforcement learning. *arXiv preprint arXiv:1012.2599*, 2010.

Brown, T. B., Mann, B., Ryder, N., Subbiah, M., Kaplan, J., Dhariwal, P., Neelakantan, A., Shyam, P., Sastry, G., Askell, A., Agarwal, S., Herbert-Voss, A., Krueger, G., Henighan, T., Child, R., Ramesh, A., Ziegler, D. M., Wu, J., Winter, C., Hesse, C., Chen, M., Sigler, E., Litwin, M., Gray, S., Chess, B., Clark, J., Berner, C., McCandlish, S., Radford, A., Sutskever, I., and Amodei, D. Language models are few-shot learners, 2020. URL <https://arxiv.org/abs/2005.14165>.

Chowdhury, S. R. and Gopalan, A. On kernelized multi-armed bandits. In *International Conference on Machine Learning*, pp. 844–853. PMLR, 2017.

Diessner, M., O’Connor, J., Wynn, A., Laizet, S., Guan, Y., Wilson, K., and Whalley, R. D. Investigating bayesian optimization for expensive-to-evaluate black box functions: Application in fluid dynamics. *Frontiers in Applied Mathematics and Statistics*, 8:1076296, 2022.

Forrester, A. I. and Keane, A. J. Recent advances in surrogate-based optimization. *Progress in aerospace sciences*, 45(1-3):50–79, 2009.

Forrester, A. I. J., Sóbester, A., and Keane, A. J. Multi-fidelity optimization via surrogate modelling. *Proceedings of the Royal Society A: Mathematical, Physical and Engineering Sciences*, 463(2088):3251–3269, 2007. doi: 10.1098/rspa.2007.1900. URL <https://royalsocietypublishing.org/doi/10.1098/rspa.2007.1900>.

Foumani, Z. Z., Shishehbor, M., Yousefpour, A., and Bostanabad, R. Multi-fidelity cost-aware bayesian optimization. *Computer Methods in Applied Mechanics and Engineering*, 407:115937, 2023.

Frazier, P. I. A tutorial on bayesian optimization, 2018. URL <https://arxiv.org/abs/1807.02811>.

Griffiths, R.-R. and Hernández-Lobato, J. M. Constrained bayesian optimization for automatic chemical design, 2019. URL <https://arxiv.org/abs/1709.05501>.

Iwazaki, S., Takeno, S., Tanabe, T., and Irie, M. Failure-aware gaussian process optimization with regret bounds. *Advances in Neural Information Processing Systems*, 36: 24388–24400, 2023.

Ji, W., Pan, Y., Zhu, R., and Lei, L. Multi-armed bandits with machine learning-generated surrogate rewards, 2025. URL <https://arxiv.org/abs/2506.16658>.

Kandasamy, K., Dasarathy, G., Oliva, J. B., Schneider, J., and Póczos, B. Gaussian process bandit optimisation with multi-fidelity evaluations. *Advances in neural information processing systems*, 29, 2016.

Kaplan, J., McCandlish, S., Henighan, T., Brown, T. B., Chess, B., Child, R., Gray, S., Radford, A., Wu, J., and Amodei, D. Scaling laws for neural language models. *arXiv preprint arXiv:2001.08361*, 2020.

Le Gratiet, L. Bayesian analysis of hierarchical multifidelity codes. *SIAM/ASA Journal on Uncertainty Quantification*, 1(1):244–269, 2013. doi: 10.1137/120884122. URL <https://doi.org/10.1137/120884122>.

Ludwig, J. and Mullainathan, S. Machine learning as a tool for hypothesis generation. *The Quarterly Journal of Economics*, 139(2):751–827, 2024.

McInnes, L., Healy, J., and Melville, J. Umap: Uniform manifold approximation and projection for dimension reduction, 2020. URL <https://arxiv.org/abs/1802.03426>.

Milkman, K. L., Gromet, D., Ho, H., Kay, J. S., Lee, T. W., Pandiloski, P., Park, Y., Rai, A., Bazerman, M., Beshears, J., et al. Megastudies improve the impact of applied behavioural science. *Nature*, 600(7889):478–483, 2021.

OpenAI. o4-mini model documentation. <https://platform.openai.com/docs/models/o4-mini>, 2025. Accessed 2026-01-27.

Peherstorfer, B., Willcox, K., and Gunzburger, M. Survey of multifidelity methods in uncertainty propagation, inference, and optimization. *SIAM Review*, 60(3):550–591, 2018. doi: 10.1137/16M1082469. URL <https://doi.org/10.1137/16M1082469>.

Pepe, M. S. Inference using surrogate outcome data and a validation sample. *Biometrika*, 79(2):355–365, 1992.

Robins, J. M., Rotnitzky, A., and Zhao, L. P. Estimation of regression coefficients when some regressors are not always observed. *Journal of the American statistical Association*, 89(427):846–866, 1994.

Salton, G. and Buckley, C. Term-weighting approaches in automatic text retrieval. *Information Processing & Management*, 24(5):513–523, 1988. ISSN 0306-4573. doi: [https://doi.org/10.1016/0306-4573\(88\)90021-0](https://doi.org/10.1016/0306-4573(88)90021-0). URL <https://www.sciencedirect.com/science/article/pii/0306457388900210>.

Santner, T. J., Williams, B. J., Notz, W. I., and Williams, B. J. *The design and analysis of computer experiments*, volume 1. Springer, 2003.

Scharfstein, D. O., Rotnitzky, A., and Robins, J. M. Adjusting for nonignorable drop-out using semiparametric nonresponse models. *Journal of the American Statistical Association*, 94(448):1096–1120, 1999.

Shahriari, B., Swersky, K., Wang, Z., Adams, R. P., and De Freitas, N. Taking the human out of the loop: A review of bayesian optimization. *Proceedings of the IEEE*, 104(1):148–175, 2015.

Snoek, J., Larochelle, H., and Adams, R. P. Practical bayesian optimization of machine learning algorithms. In Pereira, F., Burges, C., Bottou, L., and Weinberger, K. (eds.), *Advances in Neural Information Processing Systems*, volume 25. Curran Associates, Inc., 2012. URL https://proceedings.neurips.cc/paper_files/paper/2012/file/05311655a15b75fab86956663e1819cd-Paper.pdf.

Srinivas, N., Krause, A., Kakade, S., and Seeger, M. Gaussian process optimization in the bandit setting: No regret and experimental design. In *Proceedings of the 27th International Conference on Machine Learning (ICML)*, 2010. URL <https://arxiv.org/abs/0912.3995>.

Swersky, K., Snoek, J., and Adams, R. P. Multi-task bayesian optimization. *Advances in neural information processing systems*, 26, 2013.

Vershynin, R. *High-dimensional probability*, 2009.

Wang, Z., Dahl, G. E., Swersky, K., Lee, C., Nado, Z., Gilmer, J., Snoek, J., and Ghahramani, Z. Pre-trained gaussian processes for bayesian optimization. *Journal of Machine Learning Research*, 25(212):1–83, 2024.

Williams, C. K. and Rasmussen, C. E. *Gaussian processes for machine learning*, volume 2. MIT press Cambridge, MA, 2006.

Yan, Y., Rosales, R., Fung, G., Farooq, F., Rao, B., and Dy, J. Active learning from multiple knowledge sources. In *Artificial Intelligence and Statistics*, pp. 1350–1357. PMLR, 2012.

Yang, C., Wang, X., Lu, Y., Liu, H., Le, Q. V., Zhou, D., and Chen, X. Large language models as optimizers, 2024. URL <https://arxiv.org/abs/2309.03409>.

Zhou, Y., Liu, H., Srivastava, T., Mei, H., and Tan, C. Hypothesis generation with large language models. In *Proceedings of the 1st Workshop on NLP for Science (NLP4Science)*, pp. 117–139. Association for Computational Linguistics, 2024. doi: 10.18653/v1/2024.nlp4science-1.10. URL <http://dx.doi.org/10.18653/v1/2024.nlp4science-1.10>.

A. Related Work

The classical Gaussian Process Upper Confidence Bound (GP-UCB) algorithm is proposed in (Srinivas et al., 2010), which gives a $\mathcal{O}(\sqrt{dT\gamma_T})$ regret bound, with improvements and variations studied in (Chowdhury & Gopalan, 2017). GP-UCB is a Upper Confidence Bound (UCB)-style Bayesian algorithm (Auer et al., 2002; Auer, 2002). Our work builds upon the Vanilla GP-UCB algorithm, with the addition of oracle access to a biased but correlated predicted reward model. This augmentation of the algorithm reduces the cumulative regret of GP-UCB by a constant $\in (0, 1)$. Other lines of work in Gaussian Process (GP) bandit optimization consider different oracle access models or GP-model assumptions (Iwazaki et al., 2023; Bogunovic et al., 2016), which are orthogonal to ours as we consider a setting augmented by predicted feedback.

Meanwhile, a separate line of work focuses on enhancing statistical inference and decision-making with machine-learned predictions. The Prediction-Powered Inference (PPI) framework (Angelopoulos et al., 2023) uses an offline-trained model to generate a mean predictor for bias correction. Other papers have also explored the idea of incorporating a prediction model in various inference tasks (Robins et al., 1994; Pepe, 1992; Scharfstein et al., 1999; Athey et al., 2025), where some literature refers to the prediction model as the surrogate model. This idea was extended to bandits by (Ji et al., 2025), whose Machine Learning-Assisted Upper Confidence Bound (MLA-UCB) algorithm uses an offline model to accelerate exploration in discrete multi-armed bandit problems.

While effective for inference, PPI does not address sequential decision-making or exploration in optimization problems. While MLA-UCB extends this idea to a sequential setting by incorporating machine-learned predictions into multi-armed bandits, MLA-UCB treats predictions as arm-level advice in a discrete action space and does not exploit structural or geometric relationships between arms, nor does it extend to continuous domains. PA-GP-UCB takes a different approach by integrating predictions directly into a joint Gaussian process model over high- and low-fidelity signals. The resulting covariance structure governs both exploration and interpolation in a continuous domain. Within this framework, PA-GP-UCB employs a PPI-style control-variates estimator inside the bandit algorithm, enabling principled variance reduction while supporting sample-efficient exploration.

Our work connects to recent applications of UCB-style algorithms for hypothesis generation with LLMs. Specifically, (Zhou et al., 2024) proposes a UCB-inspired method to enhance LLM-based hypothesis generation, supported by empirical experiments. This builds on growing interest in using LLMs for scientific hypothesis generation (Griffiths & Hernández-Lobato, 2019) and as prediction or surrogate models in optimization (Yang et al., 2024). Our paper formalizes the hypothesis generation process in a continuous embedding space into a mathematical framework with provable guarantees, extending the empirical findings of (Zhou et al., 2024) and providing theoretical grounding for the use of bias-corrected predictions in Bayesian optimization.

Finally, our work is also closely related but orthogonal to literature on multi-fidelity bandit algorithms (Kandasamy et al., 2016; Le Gratiet, 2013; Forrester et al., 2007; Yan et al., 2012; Swersky et al., 2013; Foumani et al., 2023). The multi-fidelity literature considers settings with multiple oracle access channels of differing costs, where they select which single fidelity to query at each round and performance is typically measured as cumulative regret normalized by total query cost (Forrester et al., 2007). Our work addresses a fundamentally different regime in which the prediction cost is negligible relative to the ground-truth oracle, justifying the simultaneous observation of both oracles at each online query. While multi-fidelity methods focus on optimizing cost allocation across fidelities, they are not designed to improve regret relative to Vanilla GP optimization when performance is measured solely by the number of high-fidelity queries. In contrast, we leverage the low-fidelity oracle as side information to tighten confidence bounds and achieve strictly improved cumulative regret under a single-fidelity evaluation budget. Finally, unlike classical multi-fidelity formulations that assume uniformly bounded bias between low- and high-fidelity evaluations, our approach imposes no such bias constraint and instead requires only nonzero correlation between the two oracle outputs.

B. Proof of Theorem 4.1

B.1. Decomposing the Estimation Error

Lemma B.1 (Error decomposition). *Conditioned on previous online queries \mathcal{D}_{t-1} , we have*

$$\mu_t^{PA}(x) - f(x) \triangleq E_1(x) + E_2(x),$$

where

$$E_1(x) = \frac{\rho_t(x)\sigma_t^{\text{true}}(x)}{\sigma_t^{\text{ML}}(x)}(\mu_t^{\text{ML,all}}(x) - f^{\text{ML}}(x)), \quad E_2(x) \sim \mathcal{N}(0, (\sigma_t^{\text{true}}(x))^2(1 - \rho_t(x)^2)),$$

and $E_1 \perp E_2 \mid \mathcal{D}_{t-1}$.

Proof. The following derivations are all conditioned on previous online queries \mathcal{D}_{t-1} , which implies the posterior estimates are conditionally deterministic at time t . The posterior distribution of the joint GP at point x is a bivariate Gaussian distribution,

$$\begin{bmatrix} f \\ f^{\text{ML}} \end{bmatrix} \sim \mathcal{N}\left(\begin{bmatrix} \mu_t^{\text{true}}(x) \\ \mu_t^{\text{ML}}(x) \end{bmatrix}, \begin{bmatrix} (\sigma_t^{\text{true}}(x))^2 & \rho_t(x)\sigma_t^{\text{ML}}(x)\sigma_t^{\text{true}}(x) \\ \rho_t(x)\sigma_t^{\text{ML}}(x)\sigma_t^{\text{true}}(x) & (\sigma_t^{\text{ML}}(x))^2 \end{bmatrix}\right).$$

Applying the conditional distribution formula of bivariate Gaussian variables, we get that,

$$f(x) \mid f^{\text{ML}}(x) = y \sim \mathcal{N}\left(\mu_t^{\text{true}}(x) + \rho_t(x)\frac{\sigma_t^{\text{true}}(x)}{\sigma_t^{\text{ML}}(x)}(y - \mu_t^{\text{ML}}(x)), (\sigma_t^{\text{true}}(x))^2(1 - \rho_t(x)^2)\right),$$

which we can rewrite as,

$$f(x) = \mu_t^{\text{true}}(x) + \rho_t(x)\frac{\sigma_t^{\text{true}}(x)}{\sigma_t^{\text{ML}}(x)}(f^{\text{ML}}(x) - \mu_t^{\text{ML}}(x)) + E_2(x),$$

where $E_2(x) \sim \mathcal{N}(0, (\sigma_t^{\text{true}}(x))^2(1 - \rho_t(x)^2))$, and $E_2(x)$ is independent to the other terms.

Therefore,

$$\mu_t^{\text{PA}}(x) - f(x) = \rho_t(x)\frac{\sigma_t^{\text{true}}(x)}{\sigma_t^{\text{ML}}(x)}(\mu_t^{\text{ML,all}}(x) - f^{\text{ML}}(x)) + E_2(x),$$

with $E_2(x)$ defined above, and is independent of the other terms conditioned on previous online queries. \square

Lemma B.2. (*Distribution of error*) Conditioned on previous online data \mathcal{D}_{t-1} , we have

$$\mu_t^{\text{PA}}(x) - f(x) \sim \mathcal{N}(0, (\sigma_t^{\text{PA}}(x))^2),$$

where

$$(\sigma_t^{\text{PA}}(x))^2 = (\sigma_t^{\text{true}}(x))^2 \left[(\rho_t(x))^2 \frac{(\sigma_t^{\text{ML,all}}(x))^2}{(\sigma_t^{\text{ML}}(x))^2} + (1 - (\rho_t(x))^2) \right] \leq (\sigma_t^{\text{true}}(x))^2.$$

Proof. We first analyze the distribution of E_1 . From Lemma B.1 we know that $E_1 = \frac{\rho_t(x)\sigma_t^{\text{true}}(x)}{\sigma_t^{\text{ML}}(x)}(\mu_t^{\text{ML,all}}(x) - f^{\text{ML}}(x))$.

The following arguments are all conditional on online data \mathcal{D}_{t-1} . Let X^{off} denote the points queried in the offline stage and $y^{\text{ML,off}} \in \mathbb{R}^{n_{\text{off}}}$ denote the offline prediction observations with $y^{\text{ML,off}} = f^{\text{ML}}(X^{\text{off}}) + \varepsilon$, $\varepsilon \sim \mathcal{N}(0, \eta_{\text{ML}}^2 I)$ independent. Define

$$\mu_t^{\text{ML,off|on}} \triangleq \mathbb{E}[y^{\text{ML,off}} \mid \mathcal{D}_{t-1}], \quad r \triangleq y^{\text{ML,off}} - \mu_t^{\text{ML,off|on}}.$$

Let

$$K(x) \triangleq \text{Cov}(f^{\text{ML}}(x), f^{\text{ML}}(X^{\text{off}}) \mid \mathcal{D}_{t-1}), \quad S \triangleq \text{Cov}(f^{\text{ML}}(X^{\text{off}}), f^{\text{ML}}(X^{\text{off}}) \mid \mathcal{D}_{t-1}) + \eta_{\text{ML}}^2 I.$$

Then $r \sim \mathcal{N}(0, S)$ and the posterior after adding \mathcal{D}^{off} satisfies

$$\mu_t^{\text{ML,all}}(x) = \mu_t^{\text{ML}}(x) + K(x)^{\top} S^{-1} r.$$

Thus,

$$\mu_t^{\text{ML,all}} - f^{\text{ML}}(x) = K(x)^{\top} S^{-1} r + (\mu_t^{\text{ML}}(x) - f^{\text{ML}}(x)).$$

Now compute the following conditional on \mathcal{D}_{t-1} ,

$$\begin{aligned}
 \text{Var}(\mu_t^{\text{ML,all}}(x) - f^{\text{ML}}(x)) &= \text{Var}(K(x)^\top S^{-1}r + \mu_t^{\text{ML}}(x) - f^{\text{ML}}(x)) \\
 &= \text{Var}(\mu_t^{\text{ML}}(x) - f^{\text{ML}}(x)) - 2\text{Cov}(\mu_t^{\text{ML}}(x) - f^{\text{ML}}(x), K(x)^\top S^{-1}r) + \text{Var}(K(x)^\top S^{-1}r) \\
 &= (\sigma_t^{\text{ML}}(x))^2 - 2K(x)S^{-1}K(x)^\top + K(x)S^{-1}SS^{-1}K(x)^\top \\
 &= (\sigma_t^{\text{ML}}(x))^2 - K(x)S^{-1}K(x)^\top.
 \end{aligned}$$

The resulting expression, by the Bayesian updating formula, is exactly $\text{Var}(f^{\text{ML}}(x) \mid \mathcal{D}_{t-1} \cup \mathcal{D}^{\text{off}}) \triangleq (\sigma_t^{\text{ML,all}}(x))^2$. Moreover, note that $\mu_t^{\text{ML,all}}(x) - f^{\text{ML}}(x)$ has mean 0 because both r and $\mu_t^{\text{ML}}(x) - f^{\text{ML}}(x)$ have mean 0.

Thus, we get that

$$E_1(x) \sim \mathcal{N}\left(0, \left[\rho_t(x)\sigma_t^{\text{true}}(x)\frac{\sigma_t^{\text{ML,all}}(x)}{\sigma_t^{\text{ML}}(x)}\right]^2\right).$$

Finally, since $E_1(x)$ and $E_2(x)$ are independent, the resulting error distribution in the Lemma follows. \square

B.2. Sufficient Conditions on Offline Data

Lemma B.3. (Requirement on offline data) Let $L = b\sqrt{\log(da/\delta)}$, and if

$$\varepsilon \leq \sqrt{\frac{(\sigma_{\min}^{\text{ML}}(T))^2 R}{2L^2 d^2}} \text{ and } N \geq \frac{2\eta_{\text{ML}}^2}{(\sigma_{\min}^{\text{ML}}(T))^2 R},$$

then with probability at least $1 - \delta$,

$$\left(\frac{\sigma_t^{\text{ML,all}}(x)}{\sigma_t^{\text{ML}}(x)}\right)^2 \leq R \quad \forall x \in \mathcal{X}, t \in [T].$$

Where

$$(\sigma_{\min}^{\text{ML}}(T))^2 \triangleq \frac{\frac{1}{1-\rho^2} + \frac{T}{\eta^2}}{\frac{T^2}{\eta_{\text{ML}}^2 \eta^2} + \left(\frac{1}{\eta_{\text{ML}}^2} + \frac{1}{\eta^2}\right) \frac{T}{K_{\min}(1-\rho^2)} + \frac{1}{K_{\min}^2}(1-\rho^2)}, \text{ and } K_{\min} \triangleq \min_x K(x, x).$$

Proof. The online stage of the algorithm collects T samples of $\{y^{\text{ML}}(x_t), y(x_t)\}_{t \in [T]}$ after running for T rounds. $\sigma_t^{\text{ML}}(x)$ is monotonically non-increasing in t for all $x \in \mathcal{X}$. Note that at any fixed point x , the minimum posterior variance after T rounds is at least as big as when all T queries are made at this point. In other words:

$$\min_x (\sigma_T^{\text{ML}}(x))^2 \geq \min_x \underbrace{\text{Var}(f^{\text{ML}}(x) \mid T \text{ samples of } [y(x), y^{\text{ML}}(x)])}_{\triangleq (\sigma^{\text{ML}}(T, x))^2}.$$

From the posterior formula, we get that

$$(\sigma^{\text{ML}}(T, x))^2 = \left[\frac{1}{K(x, x)} B^{-1} + \text{diag}\left(\frac{\eta^2}{T}, \frac{\eta_{\text{ML}}^2}{T}\right)^{-1} \right]_{2,2}^{-1}.$$

Compute the individual inverses,

$$B^{-1} = \frac{1}{1-\rho^2} \begin{bmatrix} 1 & -\rho \\ -\rho & 1 \end{bmatrix}, \quad \text{diag}\left(\frac{\eta^2}{T}, \frac{\eta_{\text{ML}}^2}{T}\right)^{-1} = \begin{bmatrix} \frac{T}{\eta^2} & 0 \\ 0 & \frac{T}{\eta_{\text{ML}}^2} \end{bmatrix}.$$

Substituting them back, we get that

$$\begin{aligned}
 \min_x (\sigma_T^{\text{ML}}(x))^2 &\geq \min_x (\sigma^{\text{ML}}(T, x))^2 \\
 &= \min_x \frac{\frac{1}{K(x, x)} \frac{1}{1-\rho^2} + \frac{T}{\eta^2}}{\left(\frac{T}{\eta_{\text{ML}}^2} + \frac{1}{K(x, x)} \frac{1}{1-\rho^2} \right) \left(\frac{T}{\eta^2} + \frac{1}{K(x, x)} \frac{1}{1-\rho^2} \right) - \left(\frac{\rho}{1-\rho^2} \right)^2} \\
 &\geq \frac{\frac{1}{1-\rho^2} + \frac{T}{\eta^2}}{\frac{T^2}{\eta_{\text{ML}}^2 \eta^2} + \left(\frac{1}{\eta_{\text{ML}}^2} + \frac{1}{\eta^2} \right) \frac{T}{K_{\min}(1-\rho^2)} + \frac{1}{K_{\min}^2}(1-\rho^2)} \triangleq (\sigma_{\min}^{\text{ML}}(T))^2,
 \end{aligned}$$

where we define $K_{\min} \triangleq \min_x K(x, x) > 0$ by assumption, and the last inequality is true from the assumption of $0 < K \leq 1$.

Now, we upper bound $(\sigma_t^{\text{ML,all}}(x))^2$. Since we cannot control what exactly is queried during the online stage of the algorithm, we use the offline stage to ensure an upper bound on it. In the offline stage, we construct an ε -net of size M over the domain \mathcal{X} , and at the center of each cell (denote cell as C_i and center as c_i) query N samples. Consider the following averaging estimator for any $x \in C_i$:

$$\hat{f}(x) = \frac{1}{N} \sum_{j=1}^N y^{\text{ML}}(c_i) = f^{\text{ML}}(c_i) + \hat{\varepsilon}, \quad \hat{\varepsilon} \sim \mathcal{N}(0, \frac{\eta_{\text{ML}}^2}{N}),$$

where $\hat{\varepsilon}$ is independent to $f^{\text{ML}}(c_i)$. We can compute the mean squared error of this estimator for all $x \in C_i$ and for all $i \in [M]$,

$$\begin{aligned}
 \text{MSE}(\hat{f}, x) &= \mathbb{E}[(\hat{f}(x) - f^{\text{ML}}(x))^2] = (f^{\text{ML}}(c_i) - f^{\text{ML}}(x))^2 + \frac{\eta_{\text{ML}}^2}{N} \\
 &\leq L^2 d^2 \varepsilon^2 + \frac{\eta_{\text{ML}}^2}{N} = b^2 \log(da/\delta) d^2 \varepsilon^2 + \frac{\eta_{\text{ML}}^2}{N}.
 \end{aligned}$$

The second inequality is conditional on L -Lipschitzness of f^{ML} and f as stated in Assumption 2.1, which happens with probability at least $1 - \delta$ when $L = b\sqrt{\log(da/\delta)}$.

It is well-known that Gaussian posterior updating of a function sampled from a zero mean GP (Kriging) is a Best Linear Unbiased Predictor (BLUP), i.e. with minimum mean squared error (Santner et al., 2003). Since we maintain the GPs during the algorithm through kriging, we get that

$$(\sigma_t^{\text{ML,all}}(x))^2 \leq (\sigma^{\text{off}}(x))^2 \leq \text{MSE}(\hat{f}, x), \quad \forall x \in \mathcal{X}, t \in [T].$$

The first inequality is true because conditioning on more data can only weakly decrease the posterior variance at all points in the domain.

The result in this Lemma then follows from combining the upper bound on $(\sigma_t^{\text{ML,all}}(x))^2$ and the lower bound on $(\sigma_t^{\text{ML}}(x))^2$. \square

B.3. Bounding the Instantaneous Regret

Lemma B.4 (Gaussian concentration). *For $\delta \in (0, 1)$ and set $\beta'_t = 2 \log(2|\mathcal{X}_t| \pi_t/\delta)$, with $\sum_{t \in [T]} \pi_t^{-1} \leq 1$ and $\pi_t > 0$. Then*

$$|f(x) - \mu_t^{\text{PA}}(x)| \leq \sqrt{\beta'_t} \sigma_t^{\text{PA}}(x) \quad \forall x \in \mathcal{X}_t \subset \mathcal{X}, \forall t \geq 1,$$

with probability at least $1 - \delta/2$.

Proof. Note that for any $z \sim \mathcal{N}(0, 1)$ (Vershynin, 2009),

$$\mathbb{P}\{|z| > c\} \leq \exp\left(-\frac{c^2}{2}\right).$$

Fix $t \in [T]$ and $x \in \mathcal{X}_t \subset \mathcal{X}$. From Lemma B.2 we know that $f - \mu_t^{\text{PA}} \mid \mathcal{D}_{t-1} \sim \mathcal{N}(0, (\sigma_t^{\text{PA}}(x))^2)$. Thus, applying the Chernoff bound, and union bounding over all points in \mathcal{X}_t , we get that

$$\mathbb{P} \left\{ \exists x \in \mathcal{X}_t : \frac{|f(x) - \mu_t^{\text{PA}}(x)|}{\sigma_t^{\text{PA}}(x)} > \sqrt{\beta'_t} \mid \mathcal{D}_{t-1} \right\} \leq |\mathcal{X}_t| \exp \left(-\frac{\beta'_t}{2} \right) \leq \frac{\delta}{2\pi_t}.$$

Further union bounding over all $t \in [T]$ gives the final result since we require that $\sum_{t \in [T]} \pi_t^{-1} \leq 1$.

□

At each round $t \in [T]$, we construct an ε -net of $\mathcal{X}_t \subset \mathcal{X}$ and leverage the Lipschitzness assumption 2.1 to upper bound the instantaneous regret. The ε -net is defined solely for the purpose of analysis. This is a technique similarly used in the analysis of (Srinivas et al., 2010), and we cite a useful result from it below.

Lemma B.5 (Srinivas et al. (2010) Lemma 5.7). *For $\delta \in (0, 1)$, set $\beta_t = 2 \log(4\pi_t/\delta) + 4d \log(dtbr \sqrt{\log(4da/\delta)})$, where $\sum_{t \geq 1} \pi_t^{-1} = 1$, $\pi_t > 0$. Construct a ε -net \mathcal{X}_t of size $|\mathcal{X}_t| = (dt^2 br \sqrt{\log(4da/\delta)})^d$. Let $[x^*]_t$ denote the closest point in \mathcal{X}_t to x^* . Then,*

$$|f(x^*) - \mu_t^{\text{PA}}([x^*]_t)| \leq \sqrt{\beta_t} \sigma_t^{\text{PA}}([x^*]_t) + \frac{1}{t^2}, \quad \forall t \in [T],$$

with probability at least $1 - \delta/2$.

Proof Sketch of Theorem B.5. We sketch out the proof of this Lemma. Readers interested in the details of the proof can refer to (Srinivas et al., 2010). We first leverage Assumption 2.1, which happens with probability at least $1 - \delta/4$ when $L = b\sqrt{\log(4da/\delta)}$. By Lipschitzness, one can determine an appropriate ε -net size $|\mathcal{X}_t|$ for each round $t \in [T]$ to upper bound the difference between $f([x^*]_t)$ and $f(x^*)$ by $1/t^2$ with high probability. We now use $\delta/4$ from Lipschitzness and $\delta/4$ from Lemma B.4 to get that the event in this Lemma happens with probability at least $1 - \delta/2$. We can also get an upper bound on β'_t from Lemma B.4 by substituting the value of $|\mathcal{X}_t|$,

$$\begin{aligned} 2 \log(4|\mathcal{X}_t|\pi_t/\delta) &= 2 \log(4\pi_t/\delta) + 2 \log(|\mathcal{X}_t|) \\ &= 2 \log(4\pi_t/\delta) + 2 \log \left(\left(dt^2 br \sqrt{\log(4da/\delta)} \right)^d \right) \leq \beta_t. \end{aligned}$$

□

Lemma B.6 (Instantaneous regret). *Set $\beta_t = 2 \log(4\pi_t/\delta) + 4d \log(dtbr \sqrt{\log(4da/\delta)})$. Where $\sum_{t \in [T]} \pi_t^{-1} \leq 1$ and $\pi_t > 0$. For each $t \in [T]$, conditioned on \mathcal{D}_{t-1} , we have*

$$r_t \leq 2\sqrt{\beta_t} \sigma_t^{\text{PA}}(x_t) + \frac{1}{t^2},$$

with probability at least $1 - \delta$.

Proof. A union bound over $\delta/2$ from Lemma B.5 and $\delta/2$ Lemma B.4 gives that both events hold with probability greater than $1 - \delta$. By definition of x_t as the maximizer of $\varphi_t(x)$, we get that with probability at least $1 - \delta$,

$$\begin{aligned} f(x_*) &\leq \mu_t^{\text{PA}}(x_*) + \sqrt{\beta_t} \sigma_t^{\text{PA}}(x_*) \\ &\leq \mu_t^{\text{PA}}([x^*]_t) + \sqrt{\beta_t} \sigma_t^{\text{PA}}([x^*]_t) + \frac{1}{t^2} \\ &\leq \mu_t^{\text{PA}}(x_t) + \sqrt{\beta_t} \sigma_t^{\text{PA}}(x_t) + \frac{1}{t^2}. \end{aligned}$$

Note that we can apply Lemma B.4 because β_t used here is bigger than β'_t in Lemma B.4. Thus,

$$\begin{aligned} r_t &= f(x_*) - f(x_t) \\ &\leq \mu_t^{\text{PA}}(x_t) - f(x_t) + \sqrt{\beta_t} \sigma_t^{\text{PA}}(x_t) + \frac{1}{t^2} \\ &\leq 2\sqrt{\beta_t} \sigma_t^{\text{PA}}(x_t) + \frac{1}{t^2}. \end{aligned}$$

□

B.4. Proof of Theorem 4.1

Proof of Theorem 4.1. For this proof, we adopt the choice of β_t from Lemma B.6. Since $\sum_{t \geq 1} \frac{1}{t^2} = \frac{\pi^2}{6}$, we choose $\pi_t = \frac{\pi^2 t^2}{6}$, which gives that $\sum_{t \in [T]} \pi_t^{-1} \leq \sum_{t \geq 1} \pi_t^{-1} = \frac{\pi^2}{6} \frac{6}{\pi^2} = 1$ as required. From Lemma B.6, we get that with probability at least $1 - \delta$,

$$\begin{aligned} R_T &= \sum_{t \in [T]} r_t = \sum_{t \in [T]} \left[2\sqrt{\beta_t} \sigma_t^{\text{PA}}(x_t) + \frac{1}{t^2} \right] \\ &\leq 2 \sqrt{\left(\sum_{t \in [T]} \beta_t \right) \left(\sum_{t \in [T]} (\sigma_t^{\text{PA}}(x_t))^2 \right)} + \frac{\pi^2}{6} \leq 2 \sqrt{T \beta_T \sum_{t \in [T]} (\sigma_t^{\text{PA}}(x_t))^2} + \frac{\pi^2}{6}. \end{aligned}$$

The first inequality is due to the Cauchy Schwartz inequality, and the last inequality is because β_t is non-decreasing in t .

The remainder of this proof focuses on upper bounding $4 \sum_{t \in [T]} (\sigma_t^{\text{PA}}(x_t))^2$. Given the assumption in the Theorem that $(\sigma_t^{\text{ML,all}}(x)/\sigma_t^{\text{ML}}(x))^2 \leq R$, we get that $(\sigma_t^{\text{PA}}(x))^2 \leq (1 - (1 - R)\rho_t^2(x))(\sigma_t^{\text{true}}(x))^2$. Thus,

$$\sum_{t \in [T]} (\sigma_t^{\text{PA}}(x_t))^2 \leq \sum_{t \in [T]} [1 - (1 - R)\rho_t^2(x_t)] (\sigma_t^{\text{true}}(x_t))^2. \quad (6)$$

We perform a residual decomposition on f in terms of two unconditionally independent Gaussian Process samples f^{ML} and ξ , with

$$f = \rho f^{\text{ML}} + \sqrt{1 - \rho^2} \xi, \quad \xi \sim \mathcal{GP}(0, K(x, x')). \quad (7)$$

From Lemma B.1, we know that $(1 - \rho_t^2(x))(\sigma_t^{\text{true}}(x))^2 = \text{Var}(f(x) \mid f^{\text{ML}}(x), \mathcal{D}_{t-1})$, combining with the residual decomposition (7),

$$\begin{aligned} (1 - \rho_t^2(x))(\sigma_t^{\text{true}}(x))^2 &= \text{Var}(\rho f^{\text{ML}}(x) + \sqrt{1 - \rho^2} \xi(x) \mid f^{\text{ML}}(x), \mathcal{D}_{t-1}) \\ &= (1 - \rho^2) \text{Var}(\xi(x) \mid f^{\text{ML}}(x), \mathcal{D}_{t-1}) \\ &\leq (1 - \rho^2) \text{Var}(\xi(x) \mid \mathcal{D}_{t-1}) = (1 - \rho^2)(\sigma_t^{\xi}(x))^2. \end{aligned}$$

The last inequality is true because additionally conditioning on $f^{\text{ML}}(x)$ can only decrease the posterior variance of ξ .

Rearranging this inequality gives

$$\sum_{t \in [T]} [1 - (1 - R)\rho_t^2(x_t)] (\sigma_t^{\text{true}}(x_t))^2 \leq \sum_{t \in [T]} (1 - \rho^2)(1 - R)(\sigma_t^{\xi}(x_t))^2 + R(\sigma_t^{\text{true}}(x_t))^2. \quad (8)$$

Now recall the definition of information gain of a sample of a Gaussian Process with observation noise of variance σ^2 and kernel $k(\cdot, \cdot)$,

$$\gamma_T(k, \sigma^2) \triangleq \max_{A \subset \mathcal{X}, |A|=T} \frac{1}{2} \log \det(I + \sigma^{-2} K_A), \quad (9)$$

where $K_A = [k(x, x')]_{x, x' \in A}$.

Note that by observing y_t^s and y_t^h , we can also indirectly observe z_t – a noisy observation of $\xi(x_t)$, where

$$z_t = \frac{y_t^h - \rho y_t^s}{\sqrt{1 - \rho^2}} = \xi(x_t) + \frac{\varepsilon_t^h - \rho \varepsilon_t^s}{\sqrt{1 - \rho^2}}.$$

Thus, the noisy observation z_t of $\xi(x_t)$ has variance $\frac{\eta^2 + \rho^2 \eta_{\text{ML}}^2}{1 - \rho^2}$.

A classical result from Lemma 5.4 in (Srinivas et al., 2010) shows that for a sample f of a Gaussian Process with kernel k and observation noise of variance σ^2 , the sum of posterior variances of f after querying an arbitrary sequence of T points $\{x_t\}_{t \in [T]}$ has the following property

$$4 \sum_{t \in [T]} (\sigma_t^f(x_t))^2 \leq C(\sigma^2) \gamma_T(k, \sigma^2), \quad C(\sigma^2) = \frac{8}{\log(1 + \sigma^{-2})}.$$

Let $\tilde{\sigma}_t^{\text{true}}(x)$ be the posterior standard deviation of f under a single-output GP observing only the ground-truth oracle but not the prediction oracle. Since conditioning on extra data can only reduce the posterior variance, we get that

$$\sigma_t^{\text{true}}(x_t) \leq \tilde{\sigma}_t^{\text{true}}(x_t) \quad \forall x \in \mathcal{X}, t \in [T].$$

Applying this result and Lemma 5.4 in (Srinivas et al., 2010) gives that

$$4 \sum_{t \in [T]} (\sigma_t^{\text{true}}(x_t))^2 \leq 4 \sum_{t \in [T]} (\tilde{\sigma}_t^{\text{true}}(x_t))^2 \leq C(\eta^2) \gamma_T(k, \eta^2) \stackrel{(a)}{\leq} C\left(\frac{\eta^2 + \rho^2 \eta_{\text{ML}}^2}{1 - \rho^2}\right) \underbrace{\gamma_T(k, \eta^2)}_{\triangleq \gamma_T}, \quad (10)$$

and

$$4 \sum_{t \in [T]} \sigma_t^{\xi}(x_t)^2 \leq C\left(\frac{\eta^2 + \rho^2 \eta_{\text{ML}}^2}{1 - \rho^2}\right) \gamma_T\left(k, \frac{\eta^2 + \rho^2 \eta_{\text{ML}}^2}{1 - \rho^2}\right) \stackrel{(b)}{\leq} C\left(\frac{\eta^2 + \rho^2 \eta_{\text{ML}}^2}{1 - \rho^2}\right) \gamma_T(k, \eta^2). \quad (11)$$

where inequalities (a) and (b) are true because $\frac{\eta^2 + \rho^2 \eta_{\text{ML}}^2}{1 - \rho^2} \geq \eta^2$ and that $\gamma_T(k, \sigma^2)$ is nonincreasing in σ when fixing k , and $C(\sigma^2)$ is increasing in σ^2 .

Substituting (10) and (11) into (8), and utilizing (6) gives that,

$$\begin{aligned} 4 \sum_{t \in [T]} (\sigma_t^{\text{PA}}(x_t))^2 &\stackrel{(6)}{\leq} \sum_{t \in [T]} [1 - (1 - R)\rho_t^2(x_t)] (\sigma_t^{\text{true}}(x_t))^2 \\ &\stackrel{(8)}{\leq} \sum_{t \in [T]} (1 - \rho^2)(1 - R)(\sigma_t^{\xi}(x_t))^2 + R(\sigma_t^{\text{true}}(x_t))^2 \\ &\stackrel{(10,11)}{\leq} \underbrace{\frac{8}{\log\left(1 + ((\eta^2 + \rho^2 \eta_{\text{ML}}^2)/(1 - \rho^2))^{-1}\right)}}_{\triangleq C_1} [(1 - (1 - R)\rho^2) \gamma_T. \end{aligned}$$

Hence, we have

$$R_T \leq \sqrt{C_1 \beta_T T [(1 - (1 - R)\rho^2) \gamma_T]} + \frac{\pi^2}{6}.$$

□

C. Useful Formulas

Throughout, let $k(\cdot, \cdot) \equiv K(\cdot, \cdot)$ be the prior scalar kernel and $B = \begin{bmatrix} 1 & \rho \\ \rho & 1 \end{bmatrix}$ the covariance matrix. The bivariate kernel is

$$K((x, i), (x', j)) = B_{ij} k(x, x'), \quad i, j \in \{\text{true, ML}\}.$$

For any set of inputs $X = \{x_1, \dots, x_n\}$ define the Gram matrix $K_{XX} \in \mathbb{R}^{n \times n}$ by $(K_{XX})_{ab} = k(x_a, x_b)$ and the cross-kernel row $k_{xX} \in \mathbb{R}^{1 \times n}$ by $(k_{xX})_a = k(x, x_a)$.

Online paired observations. At online round t , let $X_{t-1} = \{x_1, \dots, x_{t-1}\}$ and stack the paired observations as

$$y_{t-1} = \begin{bmatrix} y_{t-1} \\ y_{t-1}^{\text{ML}} \end{bmatrix} = \begin{bmatrix} y(x_1) \\ \vdots \\ y(x_{t-1}) \\ y^{\text{ML}}(x_1) \\ \vdots \\ y^{\text{ML}}(x_{t-1}) \end{bmatrix} \in \mathbb{R}^{2(t-1)}.$$

The corresponding noise covariance is

$$\Sigma_{\text{on}} = I_{t-1} \otimes \begin{bmatrix} \eta^2 & 0 \\ 0 & \eta_{\text{ML}}^2 \end{bmatrix}.$$

Define the multi-task Gram matrix

$$K_{t-1}^{\text{on}} \triangleq K_{X_{t-1} X_{t-1}} \otimes B \in \mathbb{R}^{2(t-1) \times 2(t-1)}.$$

For a test point x , define the cross-covariance

$$K_x^{\text{on}} \triangleq k_{x X_{t-1}} \otimes B \in \mathbb{R}^{2 \times 2(t-1)}, \quad K_{xx} \triangleq k(x, x) B \in \mathbb{R}^{2 \times 2}.$$

Then the online-only posterior (used for μ_t^{true} , μ_t^{ML} , σ_t^{true} , σ_t^{ML} and ρ_t) is

$$\begin{aligned} \mu_t^{\text{on}}(x) &= \mathbb{E}\left[\begin{bmatrix} f(x) \\ f^{\text{ML}}(x) \end{bmatrix} \mid \mathcal{D}_{t-1}\right] = K_x^{\text{on}} (K_{t-1}^{\text{on}} + \Sigma_{\text{on}})^{-1} y_{t-1}, \\ \Sigma_t^{\text{on}}(x) &= \text{Var}\left(\begin{bmatrix} f(x) \\ f^{\text{ML}}(x) \end{bmatrix} \mid \mathcal{D}_{t-1}\right) = K_{xx} - K_x^{\text{on}} (K_{t-1}^{\text{on}} + \Sigma_{\text{on}})^{-1} (K_x^{\text{on}})^{\top}. \end{aligned}$$

We extract

$$\mu_t^{\text{true}}(x) = [\mu_t^{\text{on}}(x)]_1, \quad \mu_t^{\text{ML}}(x) = [\mu_t^{\text{on}}(x)]_2, \quad (\sigma_t^{\text{true}}(x))^2 = [\Sigma_t^{\text{on}}(x)]_{11}, \quad (\sigma_t^{\text{ML}}(x))^2 = [\Sigma_t^{\text{on}}(x)]_{22},$$

and the posterior correlation

$$\rho_t(x) = \frac{[\Sigma_t^{\text{on}}(x)]_{12}}{\sigma_t^{\text{true}}(x) \sigma_t^{\text{ML}}(x)}.$$

Offline ML-prediction-only observations. Let $X^{\text{off}} = \{x_1^{\text{off}}, \dots, x_{n_{\text{off}}}^{\text{off}}\}$ and $y^{\text{off}} \in \mathbb{R}^{n_{\text{off}}}$ collect $y^{\text{ML}}(x_i^{\text{off}})$. Define

$$K_{\text{off}} \triangleq K_{X^{\text{off}} X^{\text{off}}} \in \mathbb{R}^{n_{\text{off}} \times n_{\text{off}}}, \quad k_{x, \text{off}} \triangleq k_{x X^{\text{off}}} \in \mathbb{R}^{1 \times n_{\text{off}}}.$$

Since the prediction marginal has covariance $k(\cdot, \cdot)$, the offline posterior for f^{ML} is the standard GP regression update:

$$\begin{aligned} \mu^{\text{off}}(x) &\triangleq \mathbb{E}[f^{\text{ML}}(x) \mid \mathcal{D}^{\text{off}}] = k_{x, \text{off}} (K_{\text{off}} + \eta_{\text{ML}}^2 I_{n_{\text{off}}})^{-1} y^{\text{off}}, \\ (\sigma^{\text{off}}(x))^2 &\triangleq \text{Var}(f^{\text{ML}}(x) \mid \mathcal{D}^{\text{off}}) = k(x, x) - k_{x, \text{off}} (K_{\text{off}} + \eta_{\text{ML}}^2 I_{n_{\text{off}}})^{-1} k_{x, \text{off}}^{\top}. \end{aligned}$$

(If the offline stage averages N duplicate prediction queries at each grid point, replace η_{ML}^2 by η_{ML}^2/N in the above.)

Augmented posterior using offline+online data. For the augmented model $\mathcal{GP}_{\text{true}, \text{ML}_{\text{all}}}$ conditioned on $\mathcal{D}^{\text{off}} \cup \mathcal{D}_{t-1}$, stack the observations as

$$y_{t-1}^{\text{all}} = \begin{bmatrix} y^{\text{off}} \\ y_{t-1}^{\text{ML}} \end{bmatrix} \in \mathbb{R}^{n_{\text{off}} + 2(t-1)}.$$

The joint covariance of y_{t-1}^{all} (before adding noise) is the block matrix

$$K_{t-1}^{\text{all}} = \begin{bmatrix} K_{\text{off}} & \rho K_{\text{off}, \text{on}} & K_{\text{off}, \text{on}} \\ \rho K_{\text{on}, \text{off}} & K_{\text{on}} & \rho K_{\text{on}} \\ K_{\text{on}, \text{off}} & \rho K_{\text{on}} & K_{\text{on}} \end{bmatrix},$$

where $K_{\text{on}} \triangleq K_{X_{t-1} X_{t-1}}$ and $K_{\text{off}, \text{on}} \triangleq K_{X^{\text{off}} X_{t-1}}$ (so $K_{\text{on}, \text{off}} = K_{\text{off}, \text{on}}^{\top}$). The corresponding noise covariance is

$$\Sigma_{\text{all}} = \text{diag}(\eta_{\text{ML}}^2 I_{n_{\text{off}}}, \eta^2 I_{t-1}, \eta_{\text{ML}}^2 I_{t-1}).$$

For a test point x , the cross-covariance between $(f(x), f^{\text{ML}}(x))$ and y_{t-1}^{all} is

$$K_x^{\text{all}} = \begin{bmatrix} \rho k_{x, \text{off}} & k_{x X_{t-1}} & \rho k_{x X_{t-1}} \\ k_{x, \text{off}} & \rho k_{x X_{t-1}} & k_{x X_{t-1}} \end{bmatrix} \in \mathbb{R}^{2 \times (n_{\text{off}} + 2(t-1))}.$$

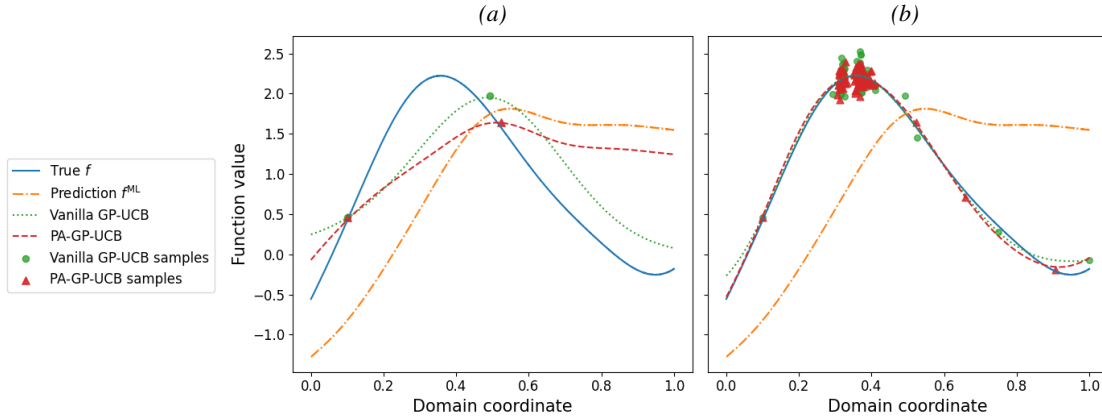


Figure 4. (a) Posterior means of Vanilla GP-UCB and PA-GP-UCB at $T = 2$ compared with the true function and the predicted function under correlation $\rho = 0.8$. (b) The corresponding posterior means at $T = 200$.

Thus the augmented posterior is

$$\begin{aligned}\mu_t^{\text{all}}(x) &= K_x^{\text{all}} (K_{t-1}^{\text{all}} + \Sigma_{\text{all}})^{-1} y_{t-1}^{\text{all}}, \\ \Sigma_t^{\text{all}}(x) &= K_{xx} - K_x^{\text{all}} (K_{t-1}^{\text{all}} + \Sigma_{\text{all}})^{-1} (K_x^{\text{all}})^{\top}.\end{aligned}$$

We extract the prediction quantities used in PA-GP-UCB as

$$\mu_t^{\text{ML,all}}(x) = [\mu_t^{\text{all}}(x)]_2, \quad (\sigma_t^{\text{ML,all}}(x))^2 = [\Sigma_t^{\text{all}}(x)]_{22}.$$

D. Additional Numerical Analysis

D.1. Posterior Visualizations

Figure 4 illustrates the evolution of the posterior under PA-GP-UCB and Vanilla GP-UCB. At $T = 1$, both methods are initialized at a random location. At $T = 2$, PA-GP-UCB exploits information from the offline prediction f^{ML} , and its posterior closely resembles the shape of the predicted function, placing its first query near the predicted optimum, even though the prediction's optimum differs from that of the true objective. As more human feedback is incorporated, the multi-task correction progressively adjusts the posterior toward the true function. By $T = 200$, the posterior under PA-GP-UCB closely matches the ground-truth function and concentrates around the true optimum, yielding an accurate reconstruction of the ground-truth function. In contrast, Vanilla GP-UCB relies solely on sparse human feedback, resulting in limited early guidance and slower convergence.

D.2. Ablations on Noise Robustness

Figure 5 reports additional ablations on observation noise and prediction noise. Figure 5(a) highlights robustness to observation noise in the true reward function. While reducing prediction noise improves performance overall, the regret gap $R_T^{\text{Vanilla}} - R_T$ shows that PA-GP-UCB yields larger gains in high-noise regimes, where reliance on expensive human feedback alone is particularly inefficient. Figure 5(b) varies the prediction noise variance η_{ML}^2 with $M = N = 1000$. PA-GP-UCB consistently outperforms Vanilla GP-UCB across all noise levels, achieving larger improvements as prediction noise decreases, while remaining robust even under highly noisy predictions.

E. LLM prediction prompting templates

This appendix lists the exact prompt templates used to query the LLM for predicting average weekly visits. In all cases, we request a single JSON number and use one deterministic query per arm.

E.1. K -shot calibrated predictions ($K = 4$ or $K = 12$)

You are predicting average weekly visits.

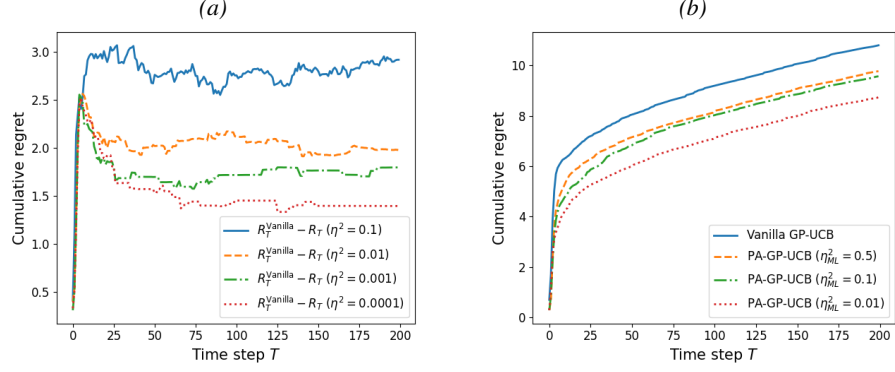


Figure 5. Cumulative regret of Vanilla GP-UCB and PA-GP-UCB averaged over 50 runs with horizon $T = 200$. (a) Regret gap $R_T^{\text{Vanilla}} - R_T$ for $\eta^2 \in \{0.1, 0.01, 0.001, 0.0001\}$ with $M = N = 1000$ and $\eta_{ML}^2 = 0.01$. (b) Effect of prediction noise, varying $\eta_{ML}^2 \in \{0.5, 0.1, 0.01\}$, with $M = N = 1000$ and $\eta^2 = 0.01$.

Here are example experimental conditions with their observed average visits:

```

1) "{cond_1}" -> {y_1:.2f}
2) "{cond_2}" -> {y_2:.2f}
...
K) "{cond_K}" -> {y_K:.2f}

```

Now predict the expected average weekly visits for:

```

"{arm_text}"

Return ONLY JSON:
{"pred_visits": number}

```

E.2. Scale-only predictions (min/max/mean only)

You are predicting average weekly visits.

Here is global context about the experiment:

- Visits are non-negative real numbers.
- Across this study, values typically range from $\{y_{\min}\}_{.1f}$ to $\{y_{\max}\}_{.1f}$.
- The average condition receives around $\{y_{\text{mean}}\}_{.1f}$ visits.
- Most conditions fall near the middle of this range.

Now predict the expected average weekly visits for:

```

"{arm_text}"

Return ONLY JSON:
{"pred_visits": number}

```

E.3. Notes on filling the template

In the scale-only prompt, $\{y_{\min}, y_{\max}, y_{\text{mean}}\}$ are computed from the set of ground-truth arm-level outcomes used for calibration and evaluation, and `arm_text` is the natural-language description of the arm. In the K -shot prompt, the pairs $\{(cond_j, y_j)\}_{j=1}^K$ are sampled from the available arm-level ground truth, with a fixed random seed for reproducibility.